EUROPEAN ORGANIZATION FOR NUCLEAR RESEARCH (CERN)

CERN-EP-2022-253
2023/02/24

CMS-B2G-21-007

Search for a vector-like quark $T' \to tH$ via the diphoton decay mode of the Higgs boson in proton-proton collisions at $\sqrt{s} = 13\,\text{TeV}$

The CMS Collaboration

Abstract

A search for the electroweak production of a vector-like quark T′, decaying to a top quark and a Higgs boson is presented. The search is based on a sample of proton-proton collision events recorded at the LHC at $\sqrt{s} = 13\,\text{TeV}$, corresponding to an integrated luminosity of $138\,\text{fb}^{-1}$. This is the first T′ search that exploits the Higgs boson decay to a pair of photons. For narrow isospin singlet T′ states with masses up to 1.1 TeV, the excellent diphoton invariant mass resolution of 1–2% results in an increased sensitivity compared to previous searches based on the same production mechanism. The electroweak production of a T′ quark with mass up to 960 GeV is excluded at 95% confidence level, assuming a coupling strength $\kappa_T = 0.25$ and a relative decay width $\Gamma / M_{T'} < 5\%$.

Submitted to the Journal of High Energy Physics

1 Introduction

The Higgs boson (H) was discovered by the ATLAS and CMS Collaborations in 2012 [1–3]. With this discovery, the standard model (SM) is now in principle complete as a low-energy effective theory, describing all known fundamental particles and their interactions. However, the stability of the Higgs boson mass at the electroweak (EW) scale remains unexplained: as the SM is extrapolated to high energies, quantum loop corrections to the Higgs boson self-energy quadratically diverge [4]. Various theories beyond the SM predict additional particles that can affect these quantum corrections to the Higgs boson mass. One such new particle is a vector-like quark (VLQ).

The VLQs are hypothetical spin-$\frac{1}{2}$, colored particles whose left- and right-handed components transform in the same way under the SM gauge group. Therefore, unlike the chiral quarks in the SM, their masses are not generated by a Yukawa coupling to the Higgs boson and have a lower contribution to the production cross section of the Higgs boson. A variety of new physics models, such as composite Higgs models [5–9], little Higgs models [10–12], and models with a warped extra dimension [13], incorporate VLQs which provide solutions to the above mentioned Higgs boson mass stability problem. In minimal models, the VLQs may only exist as electroweak singlets, denoted as T′ and B′, and doublets, carrying respective electric charges of $2/3e$ and $-1/3e$; further doublets and triplets may also exist where the VLQs can have exotic charges.

Here, we present a search for the production of a vector-like top quark partner T′ at the LHC. These could either be pair-produced by the strong interaction or singly-produced by the electroweak one. For pair production through the strong interaction, the available parton level center-of-mass energy is shared between the two heavy particles. In contrast, in the EW production of a single T′, a larger kinematic phase space is available and heavier masses can, in principle, be probed. The T′ quark can couple to SM quarks and charged or neutral bosons, resulting in decays to bW, tZ, and tH channels. For the EW production of an isospin singlet T′ VLQ, considered in this paper, the T′ branching fractions ($\mathcal{B}$) are assumed to be 50, 25, and 25%, respectively, for bW, tZ, and tH decays [14]. The leading order Feynman diagram for the electroweak T′ production along with the $\mathrm{H} \to \gamma\gamma$ decay is shown in Fig. 1. The EW production cross section depends explicitly on the couplings of the VLQ to third-generation quarks [14, 15], henceforth refered as κ_T. Here, the coupling κ_T can significantly change based on the choice of the VLQ mass and width. In this study, the VLQ production and decay are parametrized using the narrow width approximation (NWA) [16], where the T′ natural width (Γ) is approximately 1% relative to its mass ($M_{\mathrm{T}'}$). The NWA is valid up to $\Gamma/M_{\mathrm{T}'} \approx 10$–$15\%$, beyond which the large width of T′ and its interference with the SM background become important [15, 17]. However, the sensitivity of this analysis extends up to $\Gamma/M_{\mathrm{T}'} \approx 5\%$, which roughly corresponds to the experimental resolution of $M_{\mathrm{T}'}$.

This search is based on the pp collision data recorded with the CMS detector during LHC operations from 2016–2018, corresponding to an integrated luminosity of $138\,\mathrm{fb}^{-1}$. The study focuses on the EW production of T′ in proton-proton (pp) collisions at $\sqrt{s} = 13\,\mathrm{TeV}$, $\mathrm{pp} \to \mathrm{T}'\mathrm{bq}$, followed by the decay of $\mathrm{T}' \to \mathrm{tH}$, where the Higgs boson decays into a pair of photons ($\mathrm{H} \to \gamma\gamma$). The leptonic and hadronic decay modes of the top quark are treated separately to achieve the best possible search sensitivity. It is the first T′ search by the LHC experiments in $\mathrm{H} \to \gamma\gamma$ channel. The ATLAS and CMS Collaborations have previously performed searches for strong and EW production of VLQs at $\sqrt{s} = 13\,\mathrm{TeV}$ [18–23]. The most recent results on pair production [22, 23] exclude T′ masses below 1.48 TeV at 95% confidence level (CL), assuming branching fractions of 50, 25 and 25% for bW, tZ, and tH decays, respectively.

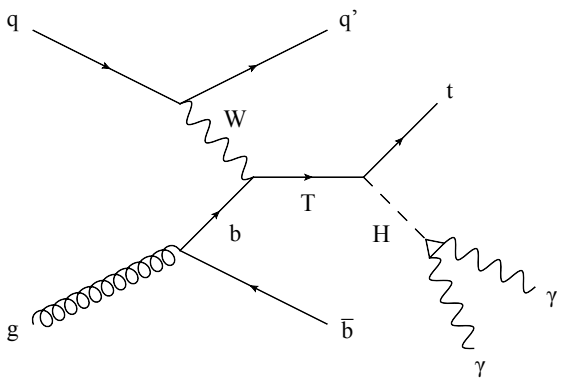

Figure 1: Leading-order Feynman diagram for single T′ production in Wb fusion and its subsequent decay into tH (H $\to \gamma\gamma$)

These previous searches used the reconstructed T′ invariant mass or transverse mass as the main observable. The present analysis exploits the excellent resolution of 1–2% for the reconstructed H mass in the diphoton decay channel to search for a signal characterized by a peak at the H mass above the falling diphoton mass ($m_{\gamma\gamma}$) continuum. The statistical methodologies and the non-Higgs background determination techniques are identical to the ones used in the SM H $\to \gamma\gamma$ measurements [24].

2 The CMS detector

The CMS apparatus [25] is a multipurpose, nearly hermetic detector, designed to trigger on [26, 27] and identify electrons, muons, photons, and charged and neutral hadrons [28–30]. A global "particle-flow" (PF) algorithm [31] aims to reconstruct all individual particles in an event, combining information provided by the all-silicon inner tracker, by the crystal electromagnetic calorimeters (ECAL), and brass-scintillator hadron calorimeters, operating inside a 3.8 T superconducting solenoid, with data from the gas-ionization muon detectors embedded in the flux-return yoke outside the solenoid. Events of interest are selected using a two-tiered trigger system. The first level of the trigger system, composed of special hardware processors, uses information from the calorimeters and muon detectors to select the most interesting events in a time interval of less than 4 μs. The second level, known as the high-level trigger, consists of a farm of processors that further decreases the event rate from around 100 kHz to less than 1 kHz [27], running a version of the full event reconstruction software optimized for fast processing. The primary vertex is taken to be the vertex corresponding to the hardest scattering in the event, evaluated using tracking information alone, as described in Section 9.4.1 of Ref. [32]. The 2017 and 2018 data sets benefit from the upgrade of the pixel tracking detector in the winter of 2016–2017 [33], improving the acceptance, redundancy, and resolution. The updated tracker greatly enhances the performance of b jet identification [34], which is essential to analysis and online event selection.

3 Simulated samples

The data analysis strategy has been optimized using Monte Carlo (MC) simulation, where specific pp event generators and a GEANT4-based detector simulation [35] have been utilized. The signal process, pp $\to$ T′($\to$ tH)bq [15], is generated to leading order and with $\Gamma/M_{\mathrm{T}'} \approx 1\%$. Samples of events are generated with MADGRAPH5_AMC@NLO 2.3.3 [36, 37]

at ten $M_{T'}$ points, from 600 to 1200 GeV, using NNPDF3.1 [38] as the parton distribution function (PDF) set. The Higgs boson and top quark masses are set to 125.0 and 172.5 GeV, respectively. The SM background processes contributing to the $m_{\gamma\gamma}$ spectrum are categorized in two types: SM Higgs boson (SMH) background and SM nonresonant background (NRB). The MADGRAPH5_aMC@NLO generator has been utilized to simulate the SM Higgs boson production, including gluon fusion (ggH) [39], vector-boson fusion (VBF) [40], production in association with top quarks (tH, $t\bar{t}H$) [41], or with a vector boson (VH) [42] at next-to-leading order in quantum chromodynamics (QCD). The total cross sections and branching fractions, as recommended by the LHC Higgs boson cross section working group [43], have been adopted for the SMH production processes. The background processes, $t + X$, $t\bar{t} + X$, $W\gamma$, and $Z\gamma$, are simulated with MADGRAPH5_aMC@NLO, whereas diboson events are produced at the leading order with PYTHIA 8.205 [44]. The nonresonant diphoton samples are simulated with SHERPA 2.2.4 [45] which includes tree-level processes with up to three additional partons, as well as box diagrams. For all MC samples, the parton showering and hadronization have been implemented via PYTHIA, with the underlying event tune CUETP8M1 [46] and CP5 [47] respectively for the 2016 and the 2017–2018 datasets. The nonresonant background samples are used to train a multivariate analysis (MVA) discriminant, while the corresponding yields are extracted using sidebands, defined by $m_{\gamma\gamma} < 115$ or $m_{\gamma\gamma} > 135$ GeV, in data.

4 Event selection

The events are selected using diphoton triggers, which require at least two photons with asymmetric conditions on the photon transverse momenta: $p_T(\gamma_1) > 30$ GeV and $p_T(\gamma_2) > 18$ or > 22 GeV, depending on the data taking period. Moreover, requirements [24] on the isolation in the calorimeter and on the shape of the electromagnetic shower are imposed. The $m_{\gamma\gamma}$ is required to be above 90 GeV, assuming both photons originate from the primary vertex.

For efficient selection of photons associated with the primary vertex a separate MVA, called the photon 'ID MVA' [24], is used based on the isolation and photon shower shape variables. Events are selected with at least two ID MVA selected photons within the ECAL and the tracker fiducial region (pseudorapidity $|\eta| < 2.5$, but excluding the ECAL barrel-endcap transition region, $1.44 < |\eta| < 1.57$). The photon pairs are further required to satisfy the criteria: $100 < m_{\gamma\gamma} < 180$ GeV, $p_T(\gamma_1)/m_{\gamma\gamma} > 1/3$, and $p_T(\gamma_2)/m_{\gamma\gamma} > 1/4$; in the case of multiple diphoton pairs, the one with highest $p_T(\gamma\gamma)$ is chosen [24].

Reconstructed particles are used to form jets using the anti-k_T algorithm with a distance parameter of 0.4 [48, 49], and to estimate the missing transverse momentum (p_T^{miss}) [50–52]. This search uses energy-corrected jet candidates with $p_T > 25$ GeV and $|\eta| < 4.5$, with stringent requirements imposed to remove spurious jets [53]. Jets must be separated from photons and leptons in the event, with $\Delta R(j,\gamma) \equiv \sqrt{(\eta_\gamma - \eta_j)^2 + (\phi_\gamma - \phi_j)^2} > 0.4$ and $\Delta R(j,\ell) > 0.4$, where ϕ is the azimuthal angle in radians. For the identification (tagging) of jets from b quark hadronization and decay (b jets), the deep neural network based DEEPCSV algorithm [54] is applied, for jets with $|\eta| < 2.5$. This search utilizes the b-tagged jets with DEEPCSV scores exceeding a minimum value corresponding to a misidentification probability of 10% for light quark and gluon jets, and to an identification efficiency for b jets of 75–90% depending on the jet p_T [54].

Isolated leptons with $p_T > 10$ GeV and within appropriate fiducial volumes ($|\eta| < 1.44$ or $1.57 < |\eta| < 2.40$, and $|\eta| < 2.40$, respectively, for electrons and muons) are considered in this search. These leptons are further required to be separated from any photon or jet considered in the analysis: $\Delta R(\ell,\gamma) > 0.4$ and $\Delta R(\ell, j) > 0.4$. Neutrinos are accounted for through the

reconstruction of $p_{\mathrm{T}}^{\mathrm{miss}}$. The $\vec{p}_{\mathrm{T}}^{\mathrm{miss}}$ vector is computed as the negative vector p_{T} sum of all the PF candidates in an event [52]. The $\vec{p}_{\mathrm{T}}^{\mathrm{miss}}$ is modified to account for corrections to the energy scale of the reconstructed jets in the event.

As mentioned above, this search categorizes events based on the leptonic or hadronic decays of the top quark. Events containing a pair of photons and at least one electron or muon are defined as the leptonic category; those with a pair of photons and no lepton form the hadronic category. To target the $\mathrm{t} \to \mathrm{bW}$ decay, at least one b-tagged jet is required in the leptonic channel, and three jets, of which at least one is b tagged, are required in the hadronic channel. Events with two leptons from the Drell–Yan processes contribute to the background in the leptonic category and are rejected by requiring $|m_{\mathrm{ee}/\mu\mu} - M_{\mathrm{Z}}| > 5\,\mathrm{GeV}$. In the leptonic category, the QCD, $\gamma +$ jets, and $\gamma\gamma +$ jets processes constitute 25% of the total background yield. In the hadronic category, however, these background contributions amount to 95% of the total. Owing to imperfect MC modelling of the $\gamma +$ jets and $\gamma\gamma +$ jets QCD processes, those backgrounds are estimated from data after reweighting the event by a cross section normalization factor. This factor is estimated by inverting the selection on the photon ID MVA, thus providing a sample of events with a significant contribution from misidentified photons.

5 Discrimination between signal and background

At this level of selection, $\mathrm{t\bar{t}H}$ with $\mathrm{H} \to \gamma\gamma$ is the dominant background among the SMH production processes for both categories, since it also leads to a peak in the $m_{\gamma\gamma}$ spectrum at the Higgs boson mass. The $m_{\gamma\gamma}$ spectrum from T' signal also peaks at M_{H} due to $\mathrm{T}' \to \mathrm{tH}$ decay. To separate the overlapping T' signal from the SMH background processes, MVA discriminants based on boosted decision trees (BDTs) are implemented [55] separately for each category (BDT-SMH). Furthermore, an additional BDT (BDT-NRB) is trained to suppress the sizeable nonresonant background contributions in the hadronic category. In the leptonic channel, discrimination against the background exploits characteristic features of the kinematic properties of each of the objects contributing to the signal (two prompt photons, b jet, lepton and neutrino) and on energy and momentum conservation. Similarly for the hadronic channel, the input features of both BDT-SMH and BDT-NRB include the kinematic properties of the physics objects: photons, jets, diphotons, reconstructed top quark candidates, jet multiplicities, $p_{\mathrm{T}}^{\mathrm{miss}}$, b-tagging scores of jets from the DeepCSV algorithm, and the output of the photon ID MVA for both photons. In order to prevent a possible correlation between $m_{\gamma\gamma}$ and the BDT score, the ratios $p_{\mathrm{T}}(\gamma_1)/m_{\gamma\gamma}$, $p_{\mathrm{T}}(\gamma_2)/m_{\gamma\gamma}$, and $p_{\mathrm{T}}(\gamma\gamma)/m_{\gamma\gamma}$ are provided as input to the BDT training, rather than using $m_{\gamma\gamma}$ directly. As the kinematic distributions of the signal vary among different $M_{\mathrm{T}'}$ values, separate BDTs have been used in three $M_{\mathrm{T}'}$ ranges: 600–700, 700–1000, and 1000–1200 GeV. In the leptonic category, the trained BDT-SMH yields a signal efficiency of more than 75%, for a background efficiency of 10%. Similarly, in the hadronic category, the trained BDT-SMH and BDT-NRB yield a signal efficiency of more than 96% and 98%, respectively, for a background efficiency of 10%. Furthermore, each of the BDT output distributions of the hadronic and leptonic categories show good agreement between data and simulation in the $m_{\gamma\gamma}$ sideband region. Figure 2 shows the distribution of the well-separated BDT output scores for signal and background processes when the training is performed over the T' samples having masses between 600 and 700 GeV

The kinematic properties of each Higgs boson candidate are always reconstructed from the momenta of the photons. However, the kinematic distributions of the top quark candidates are reconstructed differently for leptonic and hadronic channels; the leptonic channel uses constraints on the event p_{T} conservation and the W boson mass [56]; the hadronic channel uses

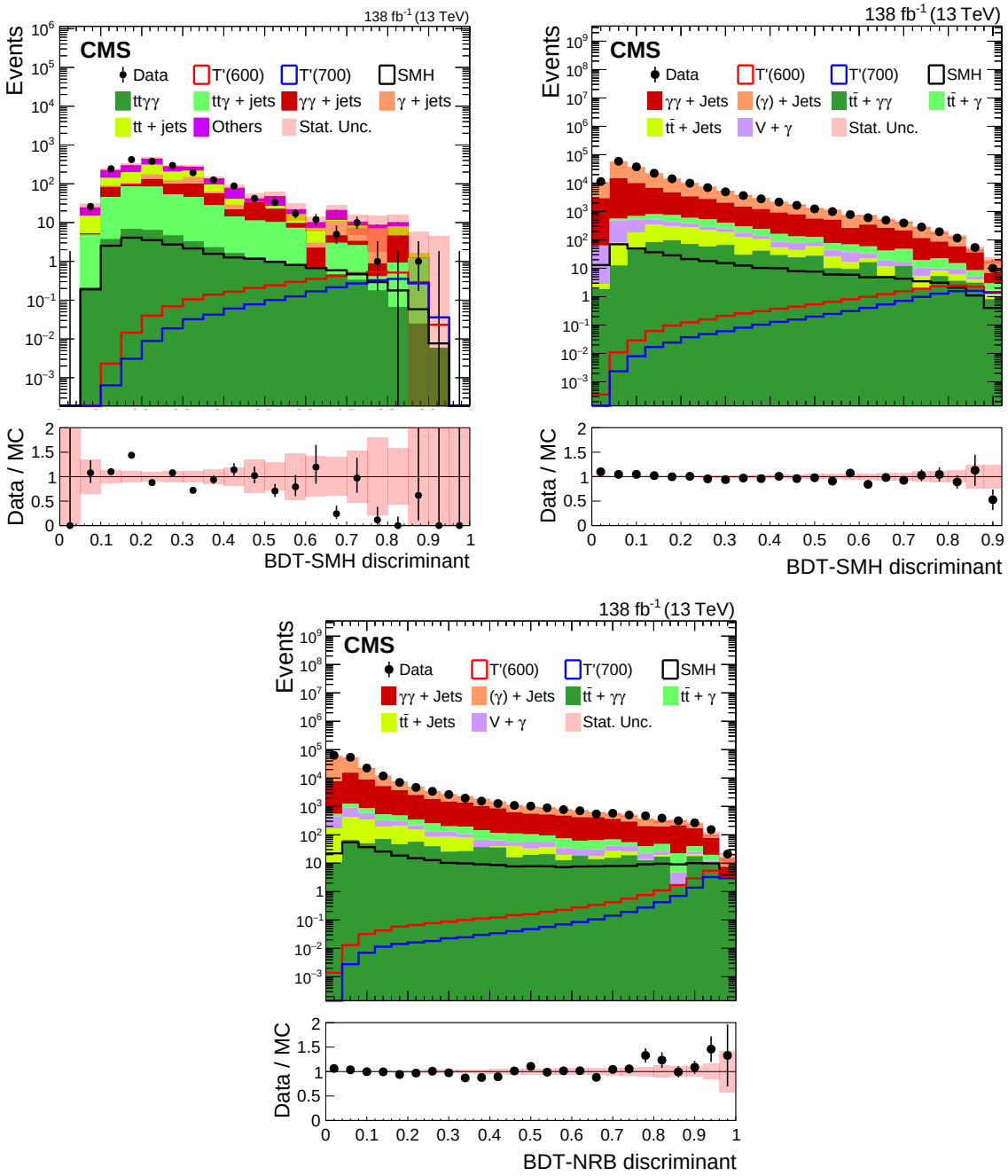

Figure 2: The BDT output distributions for data, backgrounds and signal events in the leptonic and the hadronic categories: leptonic BDT trained against the SM Higgs boson backgrounds (upper left), hadronic BDT trained against the SM Higgs boson backgrounds (upper right), and hadronic BDT trained against the nonresonant backgrounds processes (lower). For the leptonic category, MC-estimated nonresonant backgrounds are normalized to the number of observed data events. For the hadronic category, a data-driven estimation has been adapted for γ + jets backgrounds, while all other MC samples are normalized to an integrated luminosity of 138 fb^{-1}.

the minimum χ^2 method [57] to choose the correct combination of jets. The reconstructed top quark mass is also used as one of the input variables for the BDTs in the hadronic channel. The candidate T′ mass, m_{tH}, is reconstructed by combining the four-momenta of the top quark and the H candidates, with an overall experimental resolution of 5–7% in both leptonic and hadronic channels. To maximize the selection efficiency, the events considered by each optimized BDT are required to fall within a broad window in m_{tH} that extends beyond the range of $M_{\mathrm{T}'}$ for which that BDT was trained with.

The primary experimental observable for this search is the diphoton invariant mass, $m_{\gamma\gamma}$. Higgs bosons from both SM processes and T′ decay are expected to peak on a smoothly falling $m_{\gamma\gamma}$ distribution in the range $100 < m_{\gamma\gamma} < 180\,\mathrm{GeV}$. The selection criteria on the BDT discriminants for the three different $M_{\mathrm{T}'}$ ranges, labelled I, II, III in Table. 1, have been optimized to maximize signal sensitivity with respect to the background, separately for the leptonic and hadronic categories. For statistically robust modelling of the NRB from data, the optimization requires at least eight events in the signal sideband regions of $m_{\gamma\gamma}$. The m_{tH} window criterion is the same between leptonic and hadronic channels. The complete list of selection criteria on BDT score and the m_{tH} window are provided in Table. 1. The expected yield of a T′ for κ_{T} fixed at 0.2, nonresonant background, and the SM Higgs boson background processes within the signal region (SR), $m_{\gamma\gamma} \in [115, 135]\,\mathrm{GeV}$, for each signal window are shown in the Table. 2 together with the observed number of events in the SR.

Table 1: Signal selection criteria for the three BDTs and m_{tH} windows.

BDT	I	II	III
$M_{\mathrm{T}'}$(GeV)	[600, 700]	[700, 1000]	[1000, 1200]
	Hadronic analysis		
BDT-NRB score	> 0.94	>0.96	>0.95
BDT-SMH score	>0.80	>0.80	>0.80
m_{tH} window (GeV)	[480, 800]	[550, 1150]	[650, 1600]
	Leptonic analysis		
BDT score	>0.60	>0.40	>0.40
m_{tH} window (GeV)	[480, 800]	[550, 1150]	[650, 1600]

6 Signal and background modeling

Models of the signal and SMH background processes are obtained by fitting the $m_{\gamma\gamma}$ distributions in simulation with a sum of at most five Gaussian functions, separately for each category.

The models used to describe the nonresonant background processes are extracted from the observed $m_{\gamma\gamma}$ spectrum in the region $m_{\gamma\gamma} \in [100, 180]\,\mathrm{GeV}$ using a discrete profiling method [58]. This technique accounts for the systematic uncertainty in the background estimate associated with choosing a particular analytic function to describe the $m_{\gamma\gamma}$ spectrum. The chosen functions are from a list of families of functions: exponentials, power laws, polynomials, and Laurent series [58]. However, the degrees of freedom for these functions are decided in each case using a detailed $\mathcal{F}$-test [59] with a loose requirement on the goodness-of-fit.

Table 2: The expected yields of different processes in each signal window for events with a T′ with mass in the range $M_{T'} \in [600, 1200]$ GeV, and the observed number of events in the signal region $m_{\gamma\gamma} \in [115, 135]$. Here, the yields for the T′ are for κ_T fixed at 0.2.

		Leptonic yield				Hadronic yield			
BDT	$M_{T'}$ (GeV)	T′	Nonres. bkgd.	SM H bkgd.	Obs.	T′	Nonres. bkgd.	SM H bkgd.	Obs.
I	600	1.7	11.0 ± 9.0	1.3 ± 0.1	1	3.2	1.6 ± 0.9	1.8 ± 0.1	4
	625	1.7				3.5			
	650	1.6				3.6			
	675	1.6				3.7			
	700	1.5				3.6			
II	800	1.6	19.0 ± 14.4	2.3 ± 0.1	16	2.9	7.3 ± 4.0	2.0 ± 0.1	6
	900	1.2				3.0			
	1000	0.8				2.5			
III	1100	0.7	14.4 ± 13.7	1.4 ± 0.1	10	2.3	9.0 ± 5.3	2.4 ± 0.2	7
	1200	0.5				1.8			

7 Systematic uncertainties

Systematic uncertainties that modify the $m_{\gamma\gamma}$ distributions are incorporated in the signal shape and normalization as nuisance parameters. The dominant experimental uncertainties affecting the event yields and signal shape are those associated with: the integrated luminosity [60–62], the photon identification MVA ID score, the jet energy scale and resolution, the trigger efficiency, the dependence of the selection efficiency on photon shower-shape variables, the estimation of p_T^{miss}, the corrections to the photon energy scale and resolution, and the b jet identification efficiency.

In addition, theoretical uncertainties arise from the variations of the QCD renormalization and factorization scales involved in the cross section computation of the SM processes. The uncertainties that account for the limited knowledge of the PDFs and the $H \to \gamma\gamma$ branching fractions are also included. The impact of each systematic uncertainty on the final signal strength ($\mu = \sigma/\sigma_{th}$) is less than 5%, and the results are limited only by the statistical uncertainties.

8 Results

The combined (leptonic and hadronic analyses) data distributions and the corresponding signal-plus-background model fits of the $m_{\gamma\gamma}$ distribution are shown in Fig. 3 for $M_{T'}$ values of 600, 900, and 1200 GeV. No statistically significant excesses above the SM backgrounds in any of the channels or mass ranges are observed. Upper limits on the signal strength modifiers $\mu_{obs} = (\sigma)_{obs}/(\sigma)_{th}$ and $\mu_{exp} = (\sigma)_{exp}/(\sigma)_{th}$, are derived for different $M_{T'}$, using a maximum likelihood fit of the $m_{\gamma\gamma}$ distributions, keeping the M_H parameter of the model fixed at 125 GeV. The expected and observed upper limits are estimated at the 95% CL based on the CL_s criterion [63, 64] using the asymptotic approximation [65, 66] for the test statistic. The results are verified with pseudoexperiments and are cross-checked with detailed bias studies on the parameter μ.

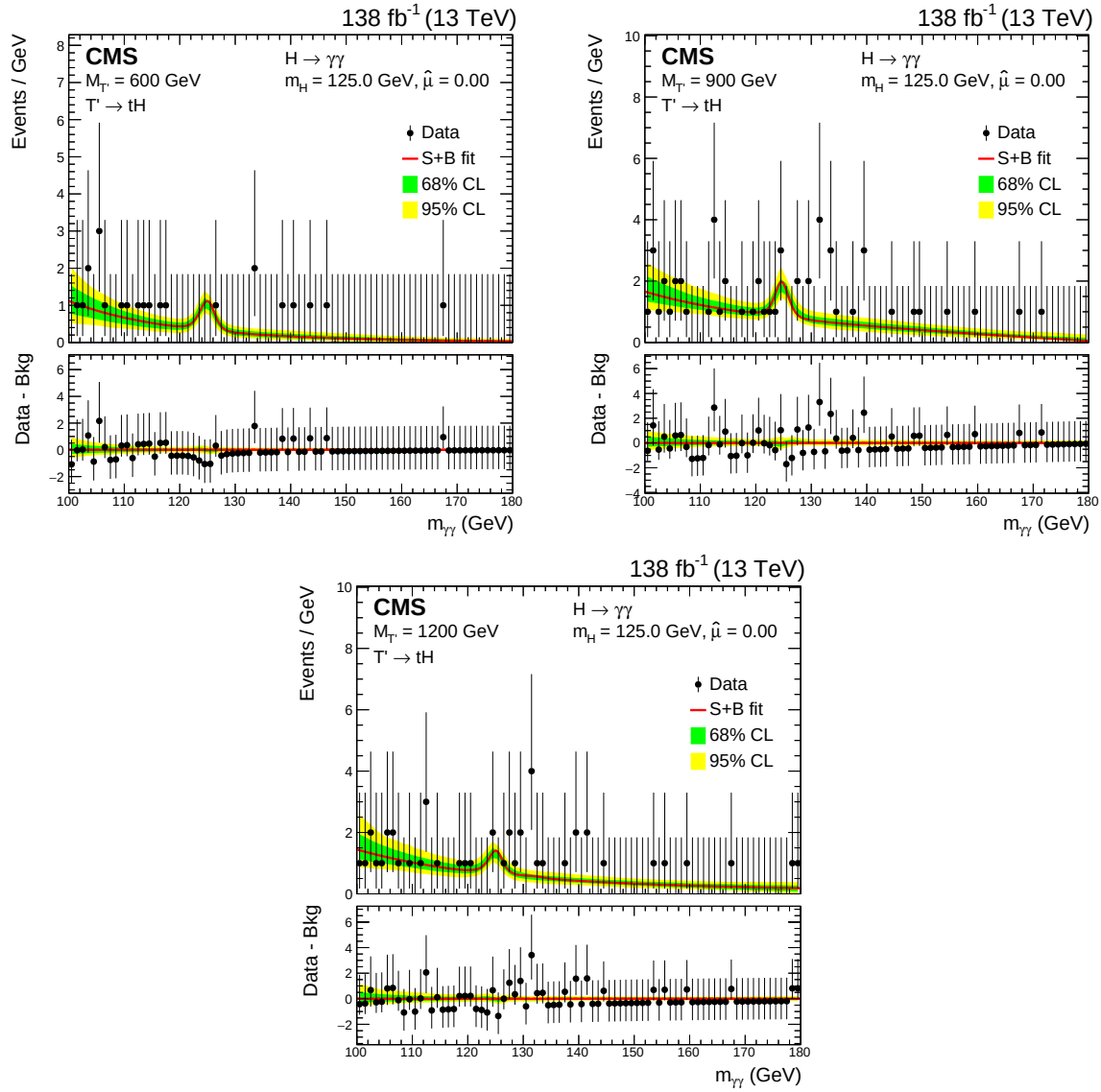

Figure 3: The combined, leptonic plus hadronic, distributions for data (black dots) and $m_{\gamma\gamma}$ signal-plus-background model fits (red line) for a VLQ signal with $M_{\mathrm{T}'}$ of 600 (upper left), 900 (upper right), and 1200 GeV (lower). The green (yellow) band represents the 68% (95%) CL in the background component of the fit. The peak in the background component shows the considered irreducible SM Higgs boson (ggH, VBF, VH, $\mathrm{t\bar{t}H}$ and tH) contribution. Here, $\hat{\mu}$ is the best fit value of the signal strength parameter μ, which is zero for the two $M_{\mathrm{T}'}$ values considered. The lower panel shows the residuals after the subtraction of the background component.

Finally, the upper limits on μ_{obs} and μ_{exp} are translated into the upper limits on $\sigma_{T'bq}\mathcal{B}_{T'\to tH}$, as displayed in Fig. 4 together with the theoretical cross sections for the singlet T′ production with representative κ_T-values fixed at 0.1, 0.15, 0.2 and 0.25 (for $\Gamma/M_{T'} < 5\%$). Similarly, the upper limits on the coupling parameter of T′ with the SM particles (κ_T) under the narrow width approximation is displayed in Fig. 5 with theoretical κ_T-values corresponding to the $\Gamma/M_{T'}$-values fixed at 1, 2, 3, 4, and 5%. Tabulated results are provided in the HEPData record for this analysis [67].

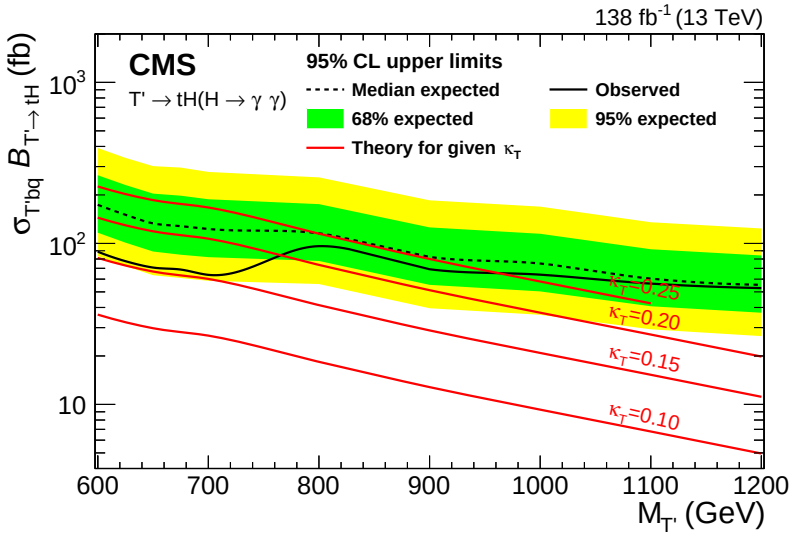

Figure 4: The combined, leptonic plus hadronic, expected (dotted black) and observed (solid black) upper limits at 95% CL on $\sigma_{T'bq}\mathcal{B}_{T'\to tH}$ are displayed as a function of $M_{T'}$. The green (yellow) band represents the 68% (95%) of the limit values expected under the background-only hypothesis. The theoretical cross sections for the singlet T′ production with representative κ_T-values fixed at 0.1, 0.15, 0.2 and 0.25 (for $\Gamma/M_{T'} < 5\%$) are shown as red lines.

9 Summary

A search for a vector-like quark decaying to a top quark and a Higgs boson that decays into two photons, T′ → tH (H → $\gamma\gamma$), has been performed using proton-proton collision data at $\sqrt{s} = 13$ TeV recorded with the CMS detector in 2016–2018, and corresponding to an integrated luminosity of 138 fb^{-1}. The search has been carried out based on a model of T′ electroweak production in a narrow width approximation with a ratio of T′ width relative to its mass ($\Gamma/M_{T'}$) $\approx 1\%$. The sensitivity of this analysis extends up to $\Gamma/M_{T'} \approx 5\%$, which roughly corresponds to the experimental resolution of $M_{T'}$. Both the hadronic and leptonic decay modes of the top quark are considered in the search. A novel multivariate analysis incorporating three separately optimized boosted decision trees is exploited to separate likely signal events from background processes, including the standard model production of Higgs bosons. No statistically significant excess over the expected background prediction is observed. Assuming a coupling to third generation quarks of $\kappa_T = 0.25$ and a relative decay width of $\Gamma/M_{T'} < 5\%$, the electroweak production of a singlet T′ quark is excluded up to a mass of 960 GeV at 95% confidence level. This search for a vector-like quark, T′, is the most sensitive to date for $M_{T'}$ up to 1.1 TeV, among searches exploring the same production mechanism.

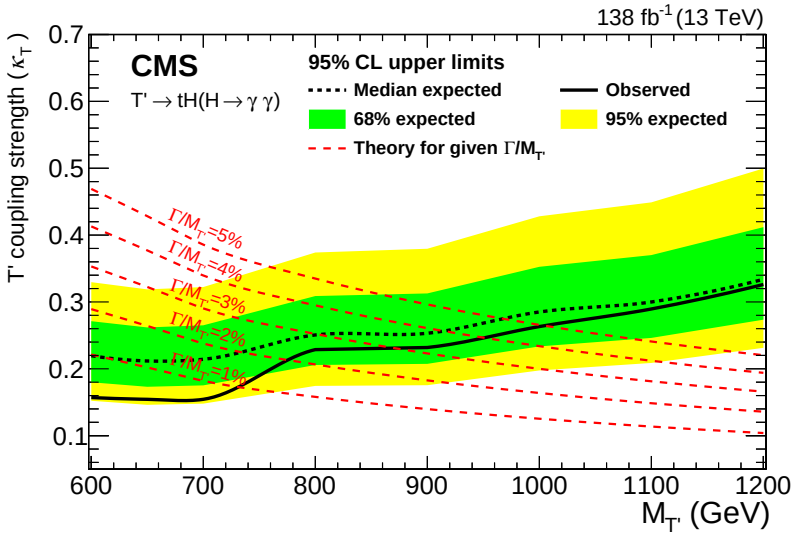

Figure 5: The combined, leptonic plus hadronic, expected (dotted black) and observed (solid black) upper limits at 95% CL on the T′ coupling to third-generation quarks, κ_T, under the narrow width approximation displayed as a function of $M_{T'}$. The green (yellow) band represents the 68% (95%) of the limit values expected under the background-only hypothesis. The theoretical κ_T values corresponding to the $\Gamma/M_{T'}$-values fixed at 1, 2, 3, 4, and 5% are shown as red dashed lines.

References

[1] ATLAS Collaboration, "Observation of a new particle in the search for the standard model Higgs boson with the ATLAS detector at the LHC", *Phys. Lett. B* **716** (2012) 1, doi:10.1016/j.physletb.2012.08.020, arXiv:1207.7214.

[2] CMS Collaboration, "Observation of a new boson at a mass of 125 GeV with the CMS experiment at the LHC", *Phys. Lett. B* **716** (2012) 30, doi:10.1016/j.physletb.2012.08.021, arXiv:1207.7235.

[3] CMS Collaboration, "Observation of a new boson with mass near 125 GeV in pp collisions at $\sqrt{s} = 7$ and 8 TeV", *JHEP* **06** (2013) 81, doi:10.1007/JHEP06(2013)081, arXiv:1303.4571.

[4] L. Susskind, "Dynamics of spontaneous symmetry breaking in the Weinberg–Salam theory", *Phys. Rev. D* **20** (1979) 2619, doi:10.1103/PhysRevD.20.2619.

[5] R. Contino, L. Da Rold, and A. Pomarol, "Light custodians in natural composite Higgs models", *Phys. Rev. D* **75** (2007) 055014, doi:10.1103/PhysRevD.75.055014, arXiv:hep-ph/0612048.

[6] R. Contino, T. Kramer, M. Son, and R. Sundrum, "Warped/composite phenomenology simplified", *JHEP* **07** (2007) 074, doi:10.1088/1126-6708/2007/05/074, arXiv:hep-ph/0612180.

[7] D. B. Kaplan, "Flavor at SSC energies: A new mechanism for dynamically generated fermion masses", *Nucl. Phys. B* **365** (1991) 259, doi:10.1016/S0550-3213(05)80021-5.

[8] M. J. Dugan, H. Georgi, and D. B. Kaplan, "Anatomy of a composite Higgs model", *Nucl. Phys. B* **254** (1985) 299, doi:10.1016/0550-3213(85)90221-4.

[9] S. Blasi and F. Goertz, "Softened symmetry breaking in composite Higgs models", *Phys. Rev. Lett.* **123** (2019) 221801, doi:10.1103/PhysRevLett.123.221801, arXiv:1903.06146.

[10] M. Perelstein, M. E. Peskin, and A. Pierce, "Top quarks and electroweak symmetry breaking in little Higgs models", *Phys. Rev. D* **69** (2004) 075002, doi:10.1103/PhysRevD.69.075002, arXiv:hep-ph/0310039.

[11] O. Matsedonskyi, G. Panico, and A. Wulzer, "Light top partners for a light composite Higgs", *JHEP* **01** (2013) 164, doi:10.1007/JHEP01(2013)164, arXiv:1204.6333.

[12] M. Schmaltz and D. Tucker-Smith, "Little Higgs review", *Annu. Rev. Nucl. Part. Sci.* **55** (2005) 229, doi:10.1146/annurev.nucl.55.090704.151502, arXiv:hep-ph/0502182.

[13] L. Randall and R. Sundrum, "A large mass hierarchy from a small extra dimension", *Phys. Rev. Lett.* **83** (1999) 3370, doi:10.1103/PhysRevLett.83.3370, arXiv:hep-ph/9905221.

[14] J. A. Aguilar-Saavedra, R. Benbrik, S. Heinemeyer, and M. Pérez-Victoria, "Handbook of vectorlike quarks: Mixing and single production", *Phys. Rev. D* **88** (2013) 094010, doi:10.1103/PhysRevD.88.094010, arXiv:1306.0572.

[15] A. Deandrea et al., "Single production of vector-like quarks: the effects of large width, interference and NLO corrections", *JHEP* **08** (2021) 107, doi:10.1007/JHEP08(2021)107, arXiv:2105.08745.

[16] A. Roy, N. Nikiforou, N. Castro, and T. Andeen, "Novel interpretation strategy for searches of singly produced vectorlike quarks at the LHC", *Phys. Rev. D* **101** (2020) 115027, doi:10.1103/PhysRevD.101.115027, arXiv:2003.00640.

[17] S. Banerjee et al., "Phenomenological analysis of multi-pseudoscalar mediated dark matter models", *JHEP* **07** (2022) 111, doi:10.1007/JHEP07(2022)111, arXiv:2110.15391.

[18] ATLAS Collaboration, "Combination of the searches for pair-produced vector-like partners of the third-generation quarks at $\sqrt{s} = 13$ TeV with the ATLAS detector", *Phys. Rev. Lett.* **121** (2018) 211801, doi:10.1103/PhysRevLett.121.211801, arXiv:1808.02343.

[19] CMS Collaboration, "Search for pair production of vector-like quarks in the fully hadronic final state", *Phys. Rev. D* **100** (2019) 072001, doi:10.1103/PhysRevD.100.072001, arXiv:1906.11903.

[20] CMS Collaboration, "Search for electroweak production of a vector-like T quark using fully hadronic final states", *JHEP* **01** (2020) 36, doi:10.1007/JHEP01(2020)036, arXiv:1909.04721.

[21] ATLAS Collaboration, "Search for single production of a vector-like T quark decaying into a Higgs boson and top quark with fully hadronic final states using the ATLAS detector", *Phys. Rev. D* **105** (2022) 092012, doi:10.1103/PhysRevD.105.092012, arXiv:2201.07045.

[22] CMS Collaboration, "Search for pair production of vector-like quarks in leptonic final states in proton-proton collisions at $\sqrt{s} = 13\,\text{TeV}$", 2022. arXiv:2209.07327. Submitted to *JHEP*.

[23] ATLAS Collaboration, "Search for pair-produced vector-like top and bottom partners in events with large missing transverse momentum in pp collisions with the ATLAS detector", 2022. arXiv:2212.05263. Submitted to *Eur. Phy. J. C*.

[24] CMS Collaboration, "Measurements of Higgs boson production cross sections and couplings in the diphoton decay channel at $\sqrt{s} = 13\,\text{TeV}$", *JHEP* **07** (2021) 027, doi:10.1007/JHEP07(2021)027, arXiv:2103.06956.

[25] CMS Collaboration, "The CMS experiment at the CERN LHC", *JINST* **3** (2008) S08004, doi:10.1088/1748-0221/3/08/S08004.

[26] CMS Collaboration, "Performance of the CMS Level-1 trigger in proton-proton collisions at $\sqrt{s} = 13\,\text{TeV}$", *JINST* **15** (2020) P10017, doi:10.1088/1748-0221/15/10/P10017, arXiv:2006.10165.

[27] CMS Collaboration, "The CMS trigger system", *JINST* **12** (2017) P01020, doi:10.1088/1748-0221/12/01/P01020, arXiv:1609.02366.

[28] CMS Collaboration, "Electron and photon reconstruction and identification with the CMS experiment at the CERN LHC", *JINST* **16** (2021) P05014, doi:10.1088/1748-0221/16/05/p05014, arXiv:2012.06888.

[29] CMS Collaboration, "Performance of the CMS muon detector and muon reconstruction with proton-proton collisions at $\sqrt{s} = 13\,\text{TeV}$", *JINST* **13** (2018) P06015, doi:10.1088/1748-0221/13/06/p06015, arXiv:1804.04528.

[30] CMS Collaboration, "Description and performance of track and primary-vertex reconstruction with the CMS tracker", *JINST* **9** (2014) P10009, doi:10.1088/1748-0221/9/10/P10009, arXiv:1405.6569.

[31] CMS Collaboration, "Particle-flow reconstruction and global event description with the CMS detector", *JINST* **12** (2017) P10003, doi:10.1088/1748-0221/12/10/P10003, arXiv:1706.04965.

[32] CMS Collaboration, "Technical proposal for the Phase-II upgrade of the Compact Muon Solenoid", CMS Technical Proposal CERN-LHCC-2015-010, CMS-TDR-15-02, 2015.

[33] CMS Collaboration, "CMS technical design report for the pixel detector upgrade", cms technical design report, 2012. doi:10.2172/1151650.

[34] CMS Collaboration, "Performance of b tagging algorithms in proton-proton collisions at 13 TeV with Phase 1 CMS detector", CMS Detector Performance Report CMS-DP-2018-033, 2018.

[35] GEANT4 Collaboration, "GEANT4—a simulation toolkit", *Nucl. Instrum. Meth. A* **506** (2003) 250, doi:10.1016/S0168-9002(03)01368-8.

[36] J. Alwall et al., "The automated computation of tree-level and next-to-leading order differential cross sections, and their matching to parton shower simulations", *JHEP* **07** (2014) 079, doi:10.1007/JHEP07(2014)079, arXiv:1405.0301.

[37] P. Artoisenet, R. Frederix, O. Mattelaer, and R. Rietkerk, "Automatic spin-entangled decays of heavy resonances in Monte Carlo simulations", *JHEP* **03** (2013) 015, doi:10.1007/JHEP03(2013)015, arXiv:1212.3460.

[38] NNPDF Collaboration, "Parton distributions from high-precision collider data", *Eur. Phys. J. C* **77** (2017) 663, doi:10.1140/epjc/s10052-017-5199-5, arXiv:1706.00428.

[39] E. Bagnaschi, G. Degrassi, P. Slavich, and A. Vicini, "Higgs production via gluon fusion in the POWHEG approach in the SM and in the MSSM", *JHEP* **02** (2012) 088, doi:10.1007/JHEP02(2012)088, arXiv:1111.2854.

[40] P. Nason and C. Oleari, "NLO Higgs boson production via vector-boson fusion matched with shower in POWHEG", *JHEP* **02** (2010) 037, doi:10.1007/JHEP02(2010)037, arXiv:0911.5299.

[41] H. B. Hartanto, B. Jager, L. Reina, and D. Wackeroth, "Higgs boson production in association with top quarks in the POWHEG BOX", *Phys. Rev. D* **91** (2015) 094003, doi:10.1103/PhysRevD.91.094003, arXiv:1501.04498.

[42] G. Luisoni, P. Nason, C. Oleari, and F. Tramontano, "$HW^{\pm}/HZ$ + 0 and 1 jet at NLO with the POWHEG BOX interfaced to GoSam and their merging within MiNLO", *JHEP* **10** (2013) 083, doi:10.1007/JHEP10(2013)083, arXiv:1306.2542.

[43] LHC Higgs Cross Section Working Group, "Handbook of LHC Higgs Cross Sections: 4. Deciphering the nature of the Higgs sector", *CERN Yellow Rep. Monogr.* **2** (2017) doi:10.23731/CYRM-2017-002, arXiv:1610.07922.

[44] T. Sjöstrand et al., "An introduction to PYTHIA 8.2", *Comput. Phys. Commun.* **191** (2015) 159, doi:10.1016/j.cpc.2015.01.024, arXiv:1410.3012.

[45] Sherpa Collaboration, "Event generation with SHERPA 2.2", *SciPost Phys.* **7** (2019) 034, doi:10.21468/SciPostPhys.7.3.034, arXiv:1905.09127.

[46] CMS Collaboration, "Event generator tunes obtained from underlying event and multiparton scattering measurements", *Eur. Phys. J. C* **76** (2016) 155, doi:10.1140/epjc/s10052-016-3988-x, arXiv:1512.00815.

[47] CMS Collaboration, "Extraction and validation of a new set of CMS PYTHIA 8 tunes from underlying-event measurements", *Eur. Phys. J. C* **80** (2020) 4, doi:10.1140/epjc/s10052-019-7499-4, arXiv:1903.12179.

[48] M. Cacciari, G. P. Salam, and G. Soyez, "The anti-k_{T} jet clustering algorithm", *JHEP* **04** (2008) 063, doi:10.1088/1126-6708/2008/04/063, arXiv:0802.1189.

[49] M. Cacciari, G. P. Salam, and G. Soyez, "FastJet user manual", *Eur. Phys. J. C* **72** (2012) 1896, doi:10.1140/epjc/s10052-012-1896-2, arXiv:1111.6097.

[50] CMS Collaboration, "Performance of reconstruction and identification of τ leptons decaying to hadrons and ν_τ in pp collisions at $\sqrt{s} = 13\,\mathrm{TeV}$", *JINST* **13** (2018) P10005, doi:10.1088/1748-0221/13/10/P10005, arXiv:1809.02816.

[51] CMS Collaboration, "Jet energy scale and resolution in the CMS experiment in pp collisions at 8 TeV", *JINST* **12** (2017) P02014, doi:10.1088/1748-0221/12/02/P02014, arXiv:1607.03663.

[52] CMS Collaboration, "Performance of missing transverse momentum reconstruction in proton-proton collisions at $\sqrt{s} = 13$ TeV using the CMS detector", *JINST* **14** (2019) P07004, doi:10.1088/1748-0221/14/07/P07004, arXiv:1903.06078.

[53] CMS Collaboration, "Determination of jet energy calibration and transverse momentum resolution in CMS", *JINST* **6** (2011) P11002, doi:10.1088/1748-0221/6/11/P11002, arXiv:1107.4277.

[54] CMS Collaboration, "Identification of heavy-flavour jets with the CMS detector in pp collisions at 13 TeV", *JINST* **13** (2018) P05011, doi:10.1088/1748-0221/13/05/P05011, arXiv:1712.07158.

[55] H. Voss, A. Höcker, J. Stelzer, and F. Tegenfeldt, "TMVA, the toolkit for multivariate data analysis with ROOT", in *XIth International Workshop on Advanced Computing and Analysis Techniques in Physics Research (ACAT)*, p. 40. 2007. arXiv:physics/0703039. [PoS(ACAT)040]. doi:10.22323/1.050.0040.

[56] CMS Collaboration, "Evidence for the associated production of a single top quark and a photon in proton-proton collisions at $\sqrt{s} = 13$ TeV", *Phys. Rev. Lett.* **121** (2018), no. 22, 221802, doi:10.1103/PhysRevLett.121.221802, arXiv:1808.02913.

[57] CMS Collaboration, "Search for the flavor-changing neutral current interactions of the top quark and the Higgs boson which decays into a pair of b quarks at $\sqrt{s} = 13$ TeV", *JHEP* **06** (2018) 102, doi:10.1007/JHEP06(2018)102, arXiv:1712.02399.

[58] P. D. Dauncey, M. Kenzie, N. Wardle, and G. J. Davies, "Handling uncertainties in background shapes: the discrete profiling method", *JINST* **10** (2015) P04015, doi:10.1088/1748-0221/10/04/P04015, arXiv:1408.6865.

[59] R. Fisher, "On the interpretation of χ^2 from contingency tables, and the calculation of p", *J. R. Stat. Soc* **85** (1922) 87, doi:10.2307/2340521.

[60] CMS Collaboration, "Precision luminosity measurement in proton-proton collisions at $\sqrt{s} = 13$ TeV in 2015 and 2016 at CMS", *Eur. Phys. J. C* **81** (2021) 800, doi:10.1140/epjc/s10052-021-09538-2, arXiv:2104.01927.

[61] CMS Collaboration, "CMS luminosity measurement for the 2017 data-taking period at $\sqrt{s} = 13$ TeV", CMS Physics Analysis Summary CMS-PAS-LUM-17-004, 2018.

[62] CMS Collaboration, "CMS luminosity measurement for the 2018 data-taking period at $\sqrt{s} = 13$ TeV", CMS Physics Analysis Summary CMS-PAS-LUM-18-002, 2019.

[63] T. Junk, "Confidence level computation for combining searches with small statistics", *Nucl. Instrum. Meth. A* **434** (1999) 435, doi:10.1016/S0168-9002(99)00498-2, arXiv:hep-ex/9902006.

[64] A. L. Read, "Presentation of search results: the CL_s technique", *J. Phys. G* **28** (2002) 2693, doi:10.1088/0954-3899/28/10/313.

[65] G. Cowan, K. Cranmer, E. Gross, and O. Vitells, "Asymptotic formulae for likelihood-based tests of new physics", *Eur. Phys. J. C* **71** (2011) 1554, doi:10.1140/epjc/s10052-011-1554-0, arXiv:1007.1727. [Erratum: doi:10.1140/epjc/s10052-013-2501-z].

[66] G. J. Feldman and R. D. Cousins, "A unified approach to the classical statistical analysis of small signals", *Phys. Rev. D* **57** (1998) 3873, doi:10.1103/PhysRevD.57.3873, arXiv:physics/9711021.

[67] HEPData record for this analysis, 2022. doi:10.17182/hepdata.134009.